March 2015

Submitted to:

NASA Innovative Advanced Concepts Program
Jason Derleth, NIAC Program Executive
Alvin Yew, NIAC Program Manager

Principal Investigator:

Prof. Joseph Wang, University of Southern California, josephjw@usc.edu

Co-Investigators:

Profs. Swomitra Mohanty, Tatjana Jevremovic, Manoranjan Misra, University of Utah

Student Participants:

Brain Franz, William Yu, University of Southern California

Steven Burnham, Travis Kink, University of Utah

Summary:

This report provides a summary of the work performed under NIAC Phase I award NNX15AL86G entitled "CubeSat with Nanostructured Sensing Instrumentation for Planetary Exploration". The objective of this research is to investigate the feasibility of an innovative, low cost, CubeSat based planetary mission concept for in situ "ground truth" analysis of small asteroids and comets. The project includes an instrument study and a mission/spacecraft design study. The instrument study concerns with the development of a new TiO_2 nanotube sensor with integrated compound semiconductor nanowires to determine surface composition element via neutron activated analysis (NAA). The mission/spacecraft design study concerns with the development of CubeSat based lander to small asteroids and comets. The Phase I study suggests that our concept is feasible and could provide significant benefit to NASA's future planetary missions. This research was carried out at the University of Southern California and the University of Utah.

I. Introduction and Concept

Understanding planetary surface composition is a primary science objective in any planetary exploration mission. Our knowledge of planetary surface composition has been obtained mostly from remote sensing. While remote sensing is very useful in providing information from a distance, it does not provide "ground truth" information. "Ground truth" information can only be obtained by conducting in-situ analysis on the surface. Currently, in-situ surface analysis requires very complex and expansive instruments and spacecraft, and has been used so far only by NASA's flagship missions. Due to both technology challenges and cost constrains, few options currently exist for "ground truth" analysis at small asteroids and comets. This severely limits our ability to explore and understand the solar system. This NIAC study proposes an innovative concept of a CubeSat based low cost planetary mission utilizing a new, miniature instrument for in situ analysis at asteroids or comets.

To a large extent, the challenges of in situ exploration come from the requirement from science instrument, which dictate the size, mass, power, and cost of the spacecraft that carrying the instrument. On the other hand, low cost CubeSats, while gaining popularity in recent years, have not been considered as viable platforms for planetary exploration. One of the main reasons for this is a lack of miniature science instruments suitable for integration with a CubeSat to create a CubeSat based mission. Hence, there is a great need to develop new, miniature instruments that may help to reduce the technical challenges and costs of planetary missions without scarifying the quality of science.

Our proposed NIAC research is illustrated in Figure I.1. We propose two concepts:
1. A new instrument using integrated compound semiconductor nanowires to determine surface composition element via Neutron Activated Analysis (NAA)
2. A CubeSat-based lander mission to deliver this instrument for ground truth analysis at asteroids and comets

The feasibility of both concepts is investigated through an instrument study and a mission/spacecraft design study.

II. Instrument Study

II.1 Background and Specific Objective

The proposed instrument concept is a nanostructured sensing platform using integrated compound semiconductor nanowires to determine surface composition element via Neutron Activated Analysis (NAA).

NAA is a nuclear process used for determining the concentration of elements in materials. The NAA works as follows: one uses a neutron source to bombard the surface with low energy neutrons. The naturally occurring isotopes that make up the sample transform into radioactive isotopes due to neutron capture. The compound nucleus that results gives off gamma rays promptly at different energy levels that are directly related to different elements in the target material. The quantity of a particular element may be measured by the intensity of the gamma ray emission that is associated with it. Figure II.1 illustrates the NAA process. NAA was first proposed as a non-destructive analysis technique for element analysis in the 1930s, and has since been applied widely in such

diverse fields as archaeology, geology, mining, soil science. The standard NAA analysis requires a room sized facility. (The top panel of Figure I.1 shows the NAA facility at University of Utah.)

The specific objective of the instrument study is to investigate the feasibility of transforming a room sized NAA facility into a chip sized miniature instrument. If this concept is viable, it could lead to the development of a new low cost, low power, low mass, and disposable instrument. We also note that that instrument would require no sample collection and preparation. Such an instrument could be potentially suitable for integration with a CubeSat-sized spacecraft.

The origin of the miniature instrument concept comes from the proposal team's recent research in fabricating nanowires and exploring the application of nanowire based sensors for radiation detection (Figure II.2). The University of Utah team has already fabricated Cadmium Zinc Telluride (CZT) nanowires and has demonstrated that these nanowires may be used to make CZT crystals to detect gamma rays [Gandhi et al. 2008] this provided us with a direction to develop this new instrument.

II.2 Summary of Phase I Instrument Study
During the Phase I study, the proposal team developed the instrument concept and carried out a preliminary instrument design. The instrument design addressed the following aspects: semiconductor material selection, detector efficiency/sensitivity, configuration, instrument packaging, portable neutron source, electronics design, power supply, and failure model. In particular, we developed and tested a prototype desktop size NAA sensor (reducing from the room size facility) using 5mm CZT crystals. Utilizing this setup, modeling and experimental studies were carried out to look at configurations for a portable NAA device with neutron sources for the instrument. Based on these results, two configurations were designed, one for surface analysis and one for deeper analysis (up to 1m) depending on the material below the neutron source. In addition to the NAA based miniature instrument concept, we also carried out some preliminary exploration of a concept of utilizing X-ray Fluorescence (XRF) in conjunction with NAA. This was added to compliment NAA where certain limitations were identified using NAA methodology alone with currently available materials.

The Phase I study suggests that the proposed NIAC concept is very promising. However, some major technological hurdles, primarily related to the available portable neutron sources and detector efficiencies, will need to be resolved in a Phase II study. This requires that a flight instrument to be developed in stages (i.e. initially with lower elements being detecting in the first design, followed by more elements being added as the technology is developed.)

II.3 Phase I Instrument Study Results
The section discusses the results from the Phase I instrument study

II.3.1 Neutron Activation Analysis (NAA)
NAA primarily exploits the (n,γ) nuclear interaction by detection of the gamma ray(s) emitted immediately after neutron absorption as in the case of Prompt Gamma Neutron Activation Analysis (PGNAA) or by detection of the gamma ray(s) emitted during the decay process toward a stable isotope as in the case of Delayed Gamma Neutron Activation Analysis (DGNAA). Thus, the probability of an isotope undergoing an (n,γ)

interaction greatly affects the sensitivity of NAA to a sample isotope. Since virtually all isotopes have a larger capture probability or cross-section for thermal neutrons than for fast neutrons, a thermal neutron source is desirable for high-sensitivity NAA. It is convenient to group isotopes by their thermal partial capture cross-sections. Mathematically, this is expressed as

$$\sigma_\gamma^Z(E_\gamma) = \theta P(E_\gamma, 2,200) \sigma_\gamma(2,200) \qquad (1)$$

where $\sigma_\gamma^Z(E_\gamma)$ is the thermal partial capture cross-section for element Z with isotopic abundance θ emitting a gamma ray at energy E_γ with probability P. Since the highest probability for every neutron capture is an (n,γ) interaction, the yield of prompt gamma rays is larger than that for delayed gamma rays. For PGNAA and DGNAA performed in neutron fluxes of the same magnitude, this results in most thermal partial capture cross sections being larger for PGNAA than for DGNAA [IAEA, Vienna, 2007].

Figure II.3 shows the periodic table with partial capture section. The partial capture section represents the probability that a neutron will be absorbed and emit a gamma ray. Based on the capture section, the process may be able to detect over 74 trace elements in parts per billion (ppb) range. However, in an instrument, the number of elements that can be detected will be determined by the neutron flux, the detector sensitivity, and the mass of the sample material. In order to increase the number of elements that can be detected by a miniature instrument, increased neutron flux would be needed and increased detector efficiency is required. If the neutron energies can be increased in a portable source than the number elements detected can be increased.

Conventional DGNAA is sensitive to many isotopes in the ppb range since samples can be irradiated near a reactor core with fluxes six to eight orders of magnitude greater than can be achieved with radioisotope based neutron sources. Thus, this limits the sensitivity of a miniature NAA instrument with a radioisotope neutron source to the ppm range for elements with large thermal partial capture cross-sections: B, Cd, Sm, Eu, and Gd. Elements with smaller thermal partial capture cross-sections are limited to the parts-per-thousand range or less except oxygen which is undetectable by NAA. However, the NAA can be performed over the range of neutron energies. It is always a decision of which elements are of interest to be detected, and thus the neutron energy can be decided.

II.3.2 Sensor Study: Cadmium Zinc Telluride (CZT) Detectors
The interaction of radiation with detector material occurs by four different mechanisms: elastic scattering, photoelectric effect, Compton effect, and pair production. Of the four mechanisms, the photoelectric effect is considered the most effective for detector operation. The detection mechanism is based on the photoelectric effect in the detector material.

When the gamma ray interacts with the detector material, it loses its kinetic energy by creating many electron-hole pairs through Coulombic interaction with the semiconductor lattice. The number of such pairs is proportional to the energy of the gamma ray. In order to collect the electron-hole pairs, an electric field is applied across the detector material that pushes the charges to the anode or the cathode, respectively. Collection of the charge carriers at the electrode ends creates an induced charge on the electrodes. The output is a voltage pulse whose amplitude is proportional to the charge and the deposited photon energy. A pulse height spectrum can be created. The peaks in the spectrum correspond to

the energies of the incident radiation which is unique for different elements in the material in NAA analysis. A range of compound semiconductor materials may be used as the detector material.

The proposal team has studied a variety of semiconductor materials as candidate detector materials during the Phase I. As with most gamma ray spectroscopy, detector systems with high-resolution capability and preferably high peak-to-Compton ratios are required to distinguish between energy peaks. Conventional NAA is most commonly done with High Purity Germanium (HPGe) detectors. However, due to size and complexity limitations in the CubeSat application Cadmium Zinc Telluride (CZT) detectors were considered because of their similar resolution to HPGe detectors and ability to function at room temperature [Schlesinger et al. 2001]. Figure II.4 shows a gamma ray spectrum measured from a 5mm CZT crystal at UU. The efficiency and performance of a 5mm thick CZT crystal gives a real world reference point for picking up elements from the period table

Although significant progress has been made in CZT crystal growth over the past two decades, major hurdles still exist which prevent growth of large monolithic volume detectors. Furthermore, the problem of charge trapping within single crystal grains is worsened for larger volume crystals [Prokesch 2015]. Small CZT crystal volume greatly limits the photo-peak efficiency and results in lower NAA system sensitivity than for NAA performed with HPGe detectors. However, constructing CZT crystal nanostructures could solve this problem as the high surface structure lends itself well to increased efficiency due the increased interaction between gamma rays and nanomaterial.

II.3.3 Experiment to Test the CZT Range
A 5 mm cubed planar spectrometer grade crystal was used to gauge its effectiveness for gamma ray spectroscopy. The crystal was housed in an eV-480 test fixture and connected to an eV-550 charge-sensitive preamplifier. A Canberra DSA-1000 multi-channel analyzer was used to control the system and data was recorded and analyzed using Canberra's GENIE 2000 software. Equipment setup is shown in Figure II.5. Single isotope button sources of [109]Cd, ^{137}Cs, and ^{60}Co were centered and placed 10 mm from the eV-480 window and counted to obtain photo-peak intrinsic efficiency which is shown in Figure II.6a. Efficiencies obtained by these measurements were approximately one tenth theoretical maximum obtained by Monte Carlo simulation with GEANT4 also shown in Figure II.6b. To bound the required operating parameters for a CubeSat NAA system counting times were estimated. The measured count rate of a prompt gamma ray of energy E_γ emitted from a capturing nuclide is given by:

$$\langle C \rangle = \frac{1}{V}\frac{m}{M} N_A \theta \int_V d^3\boldsymbol{r}\,\varepsilon(\boldsymbol{r}, E_\gamma) \times \int_0^\infty P(E_\gamma, v) n(\boldsymbol{r}, v)\sigma_\gamma(v)v\,dv \qquad (2)$$

where
V = volume of the sample
m = mass of the relevant element in the sample
M = atomic mass of element
N_A = Avogadro's number
θ = abundance of capturing isotope in the element
$\varepsilon(\boldsymbol{r}, E_\gamma)$ = detection efficiency for a prompt gamma of energy E_γ emitted at location $\boldsymbol{r}$
$P(E_\gamma, v)$ = absolute gamma ray emission probability of prompt gamma of energy E_γ emitted from a nucleus capturing a neutron of speed v

$n(\boldsymbol{r}, v)$ = time averaged neutron density per unit speed interval at location $\boldsymbol{r}$
$\sigma_\gamma(v)$ = radiative capture cross section for neutron of speed v

Eq. (2) can be simplified by matching a geometry of the sample to the sensor and assuming a uniform thermal neutron flux ϕ throughout the sample of mass m:

$$\langle C \rangle = \frac{1}{V}\frac{m}{M} N_A \phi \sigma_\gamma^Z(E_\gamma) \varepsilon_{ip}(E_\gamma) \frac{\Omega}{4\pi} \tag{3}$$

where ε_{ip} is the photo-peak intrinsic efficiency at gamma energy E_γ and Ω is the sold angle subtended by the sample to the surface of the detector. Counting times were estimated using Eq. (3) and are plotted in Figure II.4. For example, boron which has a thermal partial capture cross-section of 716 b for a gamma of 477.595 keV [IAEA 2007], counting time to reach 10,000 counts for a 10 g sample containing 1 ppm B-10 is 535 min. Therefore, the operating lifetime of the instrument must be approximately 1,000 minutes to detect ppm elements with the largest thermal partial capture cross-sections. Counting times can be reduced by increasing thermal neutron flux or the mass of the desired element, but due to limited types of neutron sources available and the difficulty of manipulating samples within a miniature instrument package, changing these parameters is unlikely. Alternatively, increasing the efficiency of the detector will also reduce counting times. Figure II.6 and Figure II.2 show the peak intrinsic efficiency and estimated PGNAA counting for elements that were measured and modelled illustrating the efficiency and counts needed for the planar CZT crystal.

Nano-structured CZT offers a solution to this problem, and will be explored in Phase II of this NAIC study [Gandhi et al. 2008, Dzurella 2008]. Problems with conventional radiation detectors include sensitivity, heating conditions, energy response, nonlinearity, polarization, non-uniform electric field, high bias voltage, and low spatial resolution. These problems generally have been overcome by creating nano structure-based configurations, and this strategy is recommended to improve CZT sensor technology.

It should be noted that a traditional CZT sensor array with coplanar crystals was included as part of NASA's Dawn Mission. The CZT sensor module experienced significant radiation damage with partial recovery by thermal annealing [Prettyman et al. 2011]. Prettyman, et al. recommend that the any CZT sensor system for space applications should incorporate an annealing system.

II.3.4 Compton Suppression Techniques
Due to the small CZT crystal sizes, peak-to-Compton ratios can be small enough that the Compton continuum significantly obscures full energy peaks especially for a source with many radioisotopes. In the design of a multi-element, coplanar-grid CZT detectors Moss, et al. addressed this problem by using a three-dimensional array of large detectors. By summing the spectra for gamma ray energies below 2 MeV good efficiency and a spectrum not complicated by a large Compton continuum can be achieved. Above 2 MeV, coincidence may be required to suppress the Compton continuum and escape peaks [Moss et al. 2001].

II.3.5 Neutron Source Selection
An ideal neutron source for the proposed miniature instrument would output a large number of neutrons which can be used to irradiate the sample and/or just the area on the

surface of the celestial body. Most terrestrial NAA is done with nuclear reactors which can provide thermal neutron fluxes in the range of 10^{11} to 10^{14} cm^{-2}s^{-1}. These large fluxes can overcome small capture cross-sections to achieve a sensitivity of ppm or ppb for most elements. Since a fission reactor source of neutrons is not feasible for the miniature NAA instrument, radioisotope sources are the best source of neutrons for portable NAA. Table II.1 provides a list of the most common radioisotope sources including their characteristics and Figure II.8 shows the neutron energy spectra for mixed sources and CF-252. We find that Cf-252 to be the best neutron source currently available because of its relatively large neutron source strength. However, it has a half-life of only 2.64 years which limits its utility to 10-15 years. For missions which require longer timespans ^{244}CmBe may be the best choice due to its 18.1 year half-life although its source strength is four orders of magnitude smaller. Although innovative, the "neutristor" developed by Elizondo-Decanini et al. at Sandia National Laboratory is not feasible since it can only be operated in microsecond pulses [Elizondo-Decanini et al. 2012].

II.3.6 Instrument Design and Performance Modeling

Preliminary instrument designs were carried out based on our Phase I study results. Recognizing that explorations of asteroids/comets may require both surface and sub-surface analysis, we completed two preliminary instrument designs. The first is a miniature instrument designed for sub-surface analysis. The second is for surface analysis. Both instruments are designed to operate with no sample preparation or manipulation. Due to an ongoing patent application, the instrument design diagrams are not included in this report. However, their size and weight estimations are shown in Tables II.2 and II.3, respectively, to demonstrate that it is feasible that the proposed instrument can be designed to fit within ½ U in a CubeSat.

With the sensing surface adjacent to the extraterrestrial surface, background space radiation is minimized due to the large solid angle of the sensor to the surface. Multiple nano-structured CZT sensor arrays contribute to the overall sensing volume of the instrument and provide redundancy and the possibility of coincidence counting for Compton suppression if necessary. An application specific integrated circuit card (ASIC) will be developed to control, record and transmit the data from the sensors. The instrument can be powered by battery or by miniature radioisotope thermoelectric generator.

Both instrument designs are highly sensitive to the amount of moderation neutrons from the radioisotope sources experience. Although the larger instrument design is more massive primarily due to the inclusion of moderator, including a known mass and thickness of hydrogen moderator increases the ability to estimate the neutron flux on the sample and subsequent counting times required to reach the desired sensitivity. The smaller instrument design relies on the sample surface itself to provide neutron moderation and is highly sensitive to the presence of hydrogen in the sample. This design, however, offers the benefit of some subsurface penetration (up to a meter depending on the surface).

We have carried out preliminary computational modeling of the instrument performance using Monte Carlo N-Particle (MCNP) transport code developed by Los Alamos National Laboratory. MCNP was also used to calculate penetration depth in a slab of water for neutrons with Cf-252 average energy 2.5 MeV. Figure II.9 shows neutrons reach thermal

energy after approximately 1 m of 20°C water. Figure II.10 shows the detector model developed based on the MCNP result.

II.3.7 Data Analysis Approach
We have adopted a data analysis approach using the automated spectrum analysis by Lee [Lee 2016]. The newly developed algorithm exploits the Moore-Penrose pseudo inverse matrix (MP_PIM) to quantitatively and qualitatively identify radionuclides for an observed pulse-height spectrum by comparing them to library spectra. In Lee's method, computed library spectra are created using the MCNP code and a Detector Response Function (DRF). The computed library spectra and measured spectra are compared using the MP_PIM algorithm and activity fractions for the measured spectra are estimated. Figure II.11a shows an example comparison of Ba-133 and Cs-137 computed and measured spectra for a Lanthanum Bromide detector. Figure II.11b shows the resulting residuals obtained if the measured radioisotope is not present in the computed library spectra, thus alerting the user to the presence of an additional radioisotope.

By modeling the detector system in MCNP and GEANT4, library spectra can be created for target radioisotopes and activity fractions can be estimated. Residual analysis can be done using the target radioisotope spectra or a background spectrum to find additional peaks indicating the presence of other radioisotopes.

II.3.8 Hybrid Instrumentation Approach
Additionally, we have also explored other instrumentation options that may be used in conjunction with the proposed miniature instrument for our CubeSat application. One such is the alpha proton X ray spectrometer (APXS) which has been incorporated into NASA space exploration since the Mars Pathfinder mission in 1996 [Rieder et al. 1997]. In addition, advancements in electronics have also made X ray fluorescence (XRF) spectrometers smaller and more sensitive. For example, Amptek Inc. sells off-the-shelf XRF components which fit the size, mass and power consumption constrains of the CubeSat application. XRF can detect elements with Z>10 to part-per-thousand sensitivity. This could lead to a hybrid instrumentation package combining XRF and NAA. In such a package, XRF could be applied first to provide a broad analysis to find out which elements may be present. If the elements that are suitable for the NAA analysis by the miniature instrument are present, one could switch to the NAA based instrument to carry out a more detailed concentration analysis.

II.4 Phase I Instrument Study Conclusion and Future Work
The Phase I instrumentation study suggests that:
- A portable, miniature instrument based on NAA and nanowire radiation sensor for surface element composition analysis is feasible in principle.
- Components for producing a prototype instrument that can fit into the volume of ⅓-U to ½-U of a CubeSat bus are either available off-the-shelf or can be fabricated by the proposal team. It seems feasible to develop a miniature instrument with a volume <1/2U, a weight of about 150g and power consumption of 200-500mW.

The Phase I instrumentation study also finds that the follow additional studies will need to be carried out in Phase II:

- One major issue discovered from the modeling studies is that standard CZT sensors are not efficient enough to detect all 74 elements as traditional NAA facilities can accomplish. Hence, more efficient CZT sensors should be explored in the form of CZT nanowire arrays (which has a high surface area sensor). The efficiencies of the nanowire array sensor would increase the number of elements that can be detected by the miniature instrument.
- Another approach to improve the performance of the instrument is to use a complimentary technology X-ray fluoroescence (XRF, already available in miniature components) in conjunction with NAA. The XRF can be used to first provide a broad qualitative coarse analysis of the target. If the elements that fall within the detection range of the miniature NAA instrument are fount by XRF, the NAA analysis can then be deployed. This suggests a hybrid NAA-XRF instrument package for practical applications.
- A technical hurdle in the operation of the device is the presence of Compton scattering which can provide excessive background noise to the sensors during operation. A major effort in Phase II is to investigate the Compton scattering suppression methods, such as the anti-coincidence method (which can be used to suppress or remove background (or unwanted) detector events from the true signal events) and the Fuzzy Logic method.

The Phase I study suggests that the instrument should be developed in stages with initial versions designed for detection of small number of elements, which can be further developed as more efficient detectors and better neutron sources with higher flux are developed.

III. Mission/Spacecraft Design Study

III.1 Background and Specific Objective
As shown by the Rosetta/Philae lander, landing on a comet or a small asteroid is extremely difficult and risky. Our NIAC miniature instrument concept suggests the possibility of an alternative, low cost approach to the exploration of small asteroids and comets. This NIAC study explores a CubeSat based lander mission concept.

CubeSats have been successfully used for a plethora of scientific experiments in space, typically used as a satellite for data collection via scientific payloads either in low Earth orbit or on the International Space Station. Recently, CubeSats are beginning to merge into the realm of space and planetary exploration as well. For instance, the Near-Earth Asteroid Scout (NEAScout) mission is a CubeSat solar sail mission to orbit a near-Earth asteroid for surface observations [McNutt et al. 2014]. The Mars Cube One (MarCO) will send two accompanying 6-U CubeSats to monitor the landing of the Mars InSight probe [Courtland 2016]. (The CubeSats in these missions are satellites, not landers.) Bridging the gap between CubeSat applications of satellite and lander could dramatically increase the applicability while reducing cost and complexity of mission and lander designs.

The specific objective of the mission/spacecraft study is to investigate the feasibility of integrating the miniature instrument with a CubeSat based lander and applying it to an asteroid or comet mission. Our proposed nano-lander can be either modified from off-

the-shelf CubeSat or custom built utilizing CubeSat components. Such landers are expected to have a size equivalent to about a 1-U (10 X 10 X 10 cm) or 2-U (10 X 10 X 20 cm) CubeSat and a mass on the order of 1kg. Our proposed mission operation scenario is to not use retropropulsion and allow uncontrolled landing on the surface. This method is valid for the application to small solar system bodies because the impact velocity is low enough so that the probe's mechanisms and payloads are still operational. We envision the following future asteroid/comet mission: nano-landers integrated with the miniature NAA instrument would be released from an asteroid-orbiting spacecraft for an "uncontrolled" descent and "hopping" landing. For sufficiently small asteroids or comets, no propulsion system is required. The descent and landing is completely determined by orbital dynamics and surface interaction. The landers settle at different locations on the surface with the correct orientation to allow the instrument to perform in-situ surface element analysis. If this concept is viable, it could lead to the development of an entirely new class of low cost missions to small asteroids and comets.

III.2 Summary of Phase I Mission/Spacecraft Design Study
During the Phase I study, the proposal team developed preliminary mission concept and carried out a preliminary lander design. The following aspects were addressed: landing technology (including the descent and landing) and lander design. The results suggest that it is feasible to develop a nano-lander based CubeSats, and that an uncontrolled descent and hopping landing represent the best approach for a low cost mission to small asteroids or comets. The Phase I study only considered these issues under generic conditions. We recognize that the mission design and lander design will be highly influenced by both the specific conditions of the mission. Thus, a more detailed study will need to be carried out. This will be an objective in the Phase II study.

III.3 Phase I Mission/Spacecraft Design Study Results
The section discusses the results from the Phase I mission/spacecraft study.

III.3.1 Survey of Previous Studies
While the concept in our NIAC proposal was conceived independently, several aspects in our concepts have been explored previously. Hence, a survey of previous relevant studies of small-body landings was first carried out.

The first of the uncontrolled descent and subsequent impact probe designed for a small body landing mission was PrOP-F on the Phobos 2 mission in 1989. Designed and empirically validated, it utilized a pair of level arms to upright itself once on the surface and a piston mechanism to "hop" to a different location (Figure III.1). It was targeted to be released by the mother spacecraft at a relative velocity of 300 cm/s and at an altitude of 1 km to the Martian moon, Phobos. However communication and control of the main spacecraft was lost prior to the deployment of PrOP-F so only the experiment data gathered may be used for future designs [Ulamec et al. 2011].

The Micro/Nano Experimental Robot Vehicle for Asteroids (MINERVA) was the next probe to become part of this class of small-body landers. It was carried on Hayabusa I, the JAXA mission to the near-Earth asteroid, 25143 Itokawa. Itokawa is an S-Type asteroid with a gravitational field on the order of 10^{-5} m/s^2 and an effective radius of about 500 m, which gives an escape velocity roughly on the order of 30-40 cm/s. MINERVA was a small cylindrical-shaped lander with a volume and mass of roughly

1130 cm^3 and 0.59 kg as seen in [Yoshimitsu et al. 2006] (Figure III.2). It was designed with a mobility mechanism that would allow it to "tumble" or "hop" along the surface of the asteroid, A single-internal flywheel that was on a rotating platform gave MINERVA mobility due to the generated torque from the flywheel that transferred to the system as a whole [Yoshimitsu et al. 2003] (Figures III.3, III.4). The rotating platform allow for directional "hops" although exact distances would vary due to varying surface composition. It was designed with a maximum "hop" speed of 9 cm/s to allow for a large safety margin with respect to Itokawa's escape velocity. The mission design was to release the probe from the mother spacecraft at a hovering altitude of 70 m and at a relative velocity of 5 cm/s via a pre-stress spring. Due to a timing error, the probe was released at an altitude of 200 m and with a lower relative velocity and therefore never reached the surface [Yoshimitsu et al. 2006]. The experimental data obtained during development and testing will serve as the baseline for the design of future small scale probes for uncontrolled landing on small solar system bodies.

Recently, a flywheel actuated mobile probe, Hedgehog, for the exploration of small solar system bodies was developed in tandem between NASA's Jet Propulsion Laboratory (JPL) and Stanford University. This design is much larger than MINERVA, with a mass of close to 10 kg and a volume on the order of 60,000 cm^3. Another drastic difference between Hedgehog and MINERVA was the addition of larger spikes/fixed legs to the external surface as seen in Figure III.4, for the purpose of protection, support, and the pivot points for mobility [Reid et al. 2014]. Although it has the same baseline mechanism for mobility, Hedgehog implemented three mutually orthogonal flywheels, (Figure III.5), that could spin independently from each other to allow for semi-controllable directional mobility similar to that of MINERVA by controlling the general orientation of the resulting torque vector [Reid et al. 2014]. Experimental data showed that the mobility of the apparatus was divided into two parts: pivoting and slipping/hopping. When the flywheels produced the maximum available torque of 0.22 Nm, this was sufficient for pivoting Hedgehog over simulated regolith and hard surfaces. Slipping and subsequent hopping occurred only at much larger torques which were achieved using a braking mechanism on the flywheels [Reid et al. 2014]. Although only tested in the terrestrial realm, the data was valuable in confirming 1) the numerical analysis which utilized a spring-damper component and Coulomb friction component to simulate the potential regolith and differentiate pivoting from slipping and hopping motions and 2) advancing the TRL for reaction wheel based mobility systems for small solar system body exploration.

Another small-body lander design with a mobility mechanism was the theoretical design of the Pico Autonomous Near-Earth Asteroid In Situ Characterizer (PANIC). This design implemented a tetrahedron-shaped lander with a mass of roughly 12 kg. A CAD model of the design can be seen in (Figures III.6, III.7). The proposed mobility mechanism was to use the foldable "pedals" around the tetrahedron housing to mechanically pivot the probe into the upright position from any angle [Schindler et al. 2011].

The most recent development in the uncontrolled landing of a probe on a small solar system body is the Mobile Asteroid Surface Scout (MASCOT) currently onboard Hayabusa II en route to asteroid 162173 Ryugu with a planned arrival and deployment in June 2018 and April 2019, respectively. This is JAXA's follow up asteroid sample return mission where a mobile lander was the secondary science objective. Ryugu is a C-Type asteroid but its size, gravitational field, and escape velocity is similar to those of Itokawa

[Tardivel et al. 2015]. MASCOT was developed and produced by the German Space Agency (DLR) in accordance with JAXA's mission parameters. It is a rectangular prism configuration that measures 30 cm X 30 cm X 20 cm with a mass of 10 kg. It is similar in configuration to what would be considered an 18-U CubeSat, shown in Figure III.8. Besides its size/mass difference from MINERVA, MASCOT will also rely completely on battery power due to lack of solar panels so it will only be operational for approximately 12 hours [Tardivel et al. 2015]. MASCOT will be deployed laterally from Hayabusa II with pre-stressed spring similar to MINERVA but the relative release velocity will be 3-4 cm/s and at an altitude of 100 m (Figure III.9)[Lange et al. 2010]. MASCOT will follow the same uncontrolled rebounding trajectory as was set for MINERVA, but the mobility mechanism that has been installed on MASCOT is different. MASCOT will use an internal, motor-driven eccentric arm that allows for both rotation to the upright orientation as well as provide enough energy for the entire probe to hop to a different location [Reill et al. 2015]. A CAD diagram of the mechanism is shown in Figure III.10. The mobility mechanism operates by creating a momentum pulse using the lever arm with a mass attached to the end. The DC motor actuates the arm to achieve the desired momentum pulse for either rotation or relocation [Grundmann et al. 2014]. The MASCOT probe was simulated in a Multibody System (MBS) to determine the behavior of the mobility system as well as coupled with two different surface feature models to simulate the surface interactions during movement. Since the data known about the target asteroid's surface is not highly constrained, these models have been considered accurate enough to sufficiently compare the results [Grundmann et al. 2014, Krenn et al. 2009]. Research into better simulations of regolith and other asteroid surface features is still needed.

The only probe to have ever successfully landed in an uncontrolled descent fashion to a small solar system body was the landing of Philae onto Comet 67P/Churyumov-Gerasimenko on November 24, 2014. Philae has a mass of around 100 kg and was deployed by the Rosetta orbiter at a relative velocity of 18.76 cm/s from a motor drive mechanism separation device [Biele et al. 2008]. Upon impact with the comet at about 1 m/s, Philae was not supposed to rebound by using a system of harpoons on its legs to anchor it to the surface. These failed due to the surface being harder than originally predicted [Biele et al. 2015].

III.3.2 CubeSat Based Lander Design
During the Phase I study, the design features of all of the landers reviewed in the last section have been analyzed carefully. Some of these are incorporated in the current design. We would like to emphasize that, while a few aspects of our concept are similar to those studied previously, the lander architecture being considered in this study is different. Apart from the different size and mass of the lander, the architecture and components of the lander considered here is based on that of CubeSats. The CubeSat apparatus is appealing due to its high TRL and off-the-shelf componentry that is readily available. This could reduce the cost of the specific lander and/or the overall cost of the mission. Lowering the complexity of the system is also advantageous for increasing the potential of a successful mission.

During the Phase I study, we carried out a preliminary design study of a CubeSat based lander integrated with the miniature instrument. In addition to fitting the instrument into the lander bus, a major requirement imposed on the design is that the lander needs to

achieve a correct orientation upon landing to allow the neutron beam from the NAA instrument aimed normally to the asteroid surface.

Several approaches that would allow the lander to achieve the correct orientation were explored during Phase I. We find that an easy method to achieve the correct landing orientation is through the use of an elongated lander configuration and a flywheel torque generation. In such an approach, the lander will have a much higher probability to settle on one of the longer faces rather than coming to rest in a vertical position after the "hopping" landing. Afterwards, the flywheel torque system would flip the lander so the desired face would be facing down towards the ground to allow the instrument operation.

The configuration of the lander was chosen to have a 2-U configuration for two main reasons. First, the combination of the electronics bay, mobility mechanism and main payload exceeds the 1-U volume constraint. Therefore, to adhere to the standard sizing commercially available for CubeSats, a 1.5-U or 2-U configuration is the next option. By choosing a 2-U, there is more available space for extra payloads or instrumentation. Second, the 2-U configuration has a higher side length ratio than the 1.5-U one. By having one dimension twice the length of the other two, it would significantly increase the probability that the lander will settle on one of longer faces.

Due to an ongoing patent application, the prototype design diagram is not included in this report. However, the packaging of the antenna, electronics bay, and the mobility mechanism were methodically positioned so once the 2-U sized lander has settled on the target surface, it will be aware of the internal positioning of the neutron source and will pivot to the correct face of the probe so that the neutron source is facing normal to the ground and the antenna is facing away from the surface in order to transmit the data acquired. The 2-U geometry also becomes very advantageous in this situation because the probe is symmetrical across the axis of rotation. This greatly simplifies the control system and the feedback loop that will govern the mobility of the lander on the target surface.

Table III.1 shows a comparison of the lander designed considered in this study with those in previous missions or previously considered designs. The concept considered here fills a niche in both mass and simplicity that has not yet been achieved.   We plan to develop and fabricate a working prototype of the 2-U sized lander in Phase II. The flywheel and the associated control system will be developed, and experiments will be carried out to verify the proposed landing orientation method. An experimental study will also be carried out to study the lander impact with simulated asteroid surfaces for characterization of surface material properties' influence on initial impact and subsequent mobility once settled.

III.3.3 Mission Design

During our Phase I study, a numerical simulation model was developed to simulate the proposed lander descent and landing. Obviously, the mission design depends on many variables such as an asteroid's size, mass, and shape; coefficient of restitution, etc. Modeling studies carried out in the Phase I study only considered a rather ideal situation to demonstrate the concept feasibility. The model will be refined in Phase II to include the gravitational field from an arbitrarily shaped asteroid.

This section describes the Phase I modeling result of lander descent and landing at a

small asteroid. Here, the asteroid body is assumed to be spherical and the local gravity is modeled as point source with a uniform bulk internal density (A gravitation model for an irregularly shaped body will be implemented into the simulation model in Phase II). Indirect observations have estimated the bulk density of some asteroids to be as low as 1,000-1,300 kg/m^3 while large monolithic bodies can be upwards of 3000 kg/m^3. The bulk density and mass distribution directly influence the gravitational field and escape velocity, calculated by the following equations:

$$M = \frac{4}{3}\pi\rho R^3 \qquad\qquad (4)$$

$$V_{esc} = \sqrt{\frac{2GM}{R}} \qquad\qquad (5)$$

where M, ρ, R are asteroid mass, bulk density, and radius, respectively. Universal gravitational constant is represented by G. An asteroid rotational period of 7.6 hours (average of observed asteroid spin rates [Pravec et al. 2007]) is incorporated to impart additional momentum of the lander upon surface collisions. Trajectories of the lander are also strongly dependent on surface topography and material properties, particularly, the elasticity and regolith coverage. In the simulation, coefficient of restitution (CoR), ε, is the parameter that distinguishes surface rebound behavior: bare rock and icy surface with ε of 0.8 − 0.9 and granular surface with ε of 0.2 − 0.4 [Supulver et al. 1995, Mangwandi et al. 2007]. While realistic coefficient of restitution are dependent on incident impact velocity and material properties, this parameter is assumed constant value of 0.5 or 0.8, to represent a dusty surface or bare, rocky surface, respectively. Additionally, the lander impacts on oblique surface, where the normal vector is randomly deviated up to 45° from nominal. It should be noted that solar radiation pressure on the lander is considered and noticeable, however, on the timescale of an asteroid impact landing, effects are relatively negligible for a CubeSat-sized lander. The code is constrained to a two-dimensional motion and utilized a particle-push scheme and all simulation time are taken to 40 hours at time steps of 0.1 second.

Numerical simulations were carried out for asteroids of size ranging from 1km to 100km. Figures III.11-III.15 show some representative trajectories of lander collisions for the case of a 1 km asteroid with a bulk density of 1600 kg/m^3, coefficient of restitution of 0.5, and initial velocities of 0.47 m/s, 0.047 m/s and 0.0047 m/s. The limiting, lander-capture case is depicted in Figure III.11 with an initial velocity of 0.47 m/s, matching the surface escape velocity, where some trajectories escape after initial impact while others are captured. Figures III.12 and III.13 illustrate that at smaller initial velocities, the lander does get captured and eventually comes to a rest on the surface. The effects of solar radiation pressure are appreciable as incident lander flight paths are displaced in the positive x-direction, parallel to incoming solar ultraviolet radiation. A close-up view of the rebounds is shown for an initial velocity of 0.0047 m/s in Figure III.13. Figures III.14 and III.17 plot the limiting capture case for asteroid size 10 km and 100 km, respectively.

Summaries of the simulation results are shown in Tables III.2-III.4, organized by asteroid sizes. All simulations have an initial lander altitude of 10 km from the surface. For each asteroid size, the bulk density ranged from 1600 to 3000 kg/m^3 for a coefficient of 0.5 and 0.8 to determine the limits of lander capture by the spherical body. The limits of capture can most conveniently be expressed as a ratio of initial velocity to the surface escape velocity (escape ratio). For all cases with a CoR of 0.5, the nanolander may be captured with an escape ratio 1.0, where initial lander velocity equals the surface escape velocity. More interesting results are evident for harder surface with a CoR of 0.8. The

nanolander is limited to an escape ratio of ~ 0.2, ~0.6, and ~ 0.9 for a 1 km asteroid, 10 km asteroid, and 100 km asteroid, respectively. These results suggest that lander capture is sensitive to local gravity and internal structure of the target body for bare and icy surface.

Additionally, the trajectory simulation results show that the proposed landing approach can be potentially applied to a wide range of asteroids or comets. The left panel of Figure III.16 shows the relation between the asteroid size and surface escape velocity for three internal bulk densities. The escape velocity serves as the limit of lander capture by the small body after surface impact. Comparing the results with the some of the known asteroids (the right panel of Figure III.16), we find that the proposed approach could be potentially applied to many different target bodies, ranging from asteroid 162173 Ryugu (0.92 km) to comet 1P/Halley (11 km) to asteroid 21 Lutetia (100 km).

As previously mentioned, small asteroid tend to be irregularly shaped due to the weak local gravity that is insufficient to form a spherical body. To improve this model for further numerical studies, an accurate gravitational model is crucial for near-surface dynamics. Previous gravitational model utilized spherical/ellipsoidal harmonics expansion series, while others implemented polyhedral definition of the small body. Spherical harmonics provide a good approximation outside of the Brillouin sphere (minimum circumscribing sphere), but accuracy diverges if the field is inside the Brillouin sphere. As a result, this approach is not suitable for irregularly shaped body, particularly for near-surface trajectories [Casotto and Musotto 2000]. Alternatively, a polyhedral gravity model can have high precision, however, must assume a constant density and can be computationally intensive [Werner and Scheeres 1997]. A method developed by Park et al. [2010] implements a finite element method for accurately modeling the gravitational field around irregularly shaped bodies with the capability to include density variations. Each spherical element will define a small section of the airless body along with a local mass density, fixed in position relative to the other elements, acting as individual point source. The advantage of utilizing a finite element model provides a straightforward computation of attraction, in addition to the forthright physical meaning for density estimation. Future studies will investigate the lander trajectory dependence on asteroidal shape, structural irregularities and variations in density with a gravitational finite element approach. Further simulations and experimental studies for impact and landing on granular/regolith surfaces are also to validate this approach.

III.4 Phase I Mission/Spacecraft Design Study Conclusion and Future Work

Phase I mission/spacecraft design study suggests that:
- It is feasible to develop CubeSat platform based lander for integration with the proposed instrument. The baseline lander with all necessary components to achieve the function of landing, orientating the instrument in the correct direction for operation, transmitting data can be designed for <2-U size and about 1kg.
- It is feasible to land the CubeSat based lander on a small asteroid or comet using the "uncontrolled" descent and "hopping" landing to deliver the payload.
- However, as the mission scenario and lander design will be sensitively influenced by the target body properties (size, mass, etc), surface interaction details (e.g. effects of coefficient of restitution, landscape, surface composition, etc.) and

mother spacecraft trajectories, the mission and spacecraft design will need to be refined by more realistic conditions and the benefits will need to be assessed through a detailed trade study, experimentation, and simulations in Phase II.

- In order to conclusively demonstrate the viability of the lander design, a prototype lander integrated with the instrument will need to be fabricated. The landing mechanism will also need to be investigated through multi-body and granular simulations and validated by experiments

IV. References

Barucci, M.A., E. Dotto, and A.C. Levasseur-Regourd, "Space missions to small bodies: asteroids and cometary nuclei," *Astron. Astrophys. Rev.*, vol. 19, no. 1, pp. 1–29, 2011.

Biele, J. et al., "Capabilities of Philae, The Rosetta Lander," *Space Science Review*, vol. 138, pp. 275–289, 2008.

Biele, J. et al., "The Landing(s) of Philae and Inferences About Comet Surface Mechanical Properties." *Cometary Science*, vol. 349, no. 9816, pp. 1–6, 2015.

Casotto, S, Musotto, S. "Methods for computing the potential of an irregular, homogeneous, solid body and its gradient," *AIAA*/AAS *Astrodynamics Specialist Conference*, Denver, CO, pp. 82–96, 2000.

Courtland, R., "Studying Mars, Inside and Out," *IEEE Spectrum*, vol. 53, no. 1, pp. 37–40, 2016.

Dzurella, P., "Electrical Characterization of Cadmium Zinc Telluride Nanowires for use as a Gamma Radiation Detector: Modeling and Experimentation," University of Nevada, Reno, 2008.

Elizondo-Decanini, J.M. et al., "Novel Surface-Mounted Neutron Generator," *IEEE Transactions on Plasma Science,* vol. 40, no. 9, 2012.

Gandhi, T., K.S. Raja, and M. Misra, "Cadmium zinc telluride (CZT) nanowire sensors for detection of low energy gamma-ray detection," *Proc. SPIE, Micro (MEMS) and Nanotechnologies for Space, Defense, and Security II*, vol. 6959, pp. 695904, 2008. doi:10.1117/12.771310

Grundmann, J. et al., "Mobile Asteroid Surface Scout (MASCOT) – Design, Development and Delivery of a Small Asteroid Lander Aboard Hayabusa 2," *4th IAA Planetary Defense Conference,* April 2015.

IAEA, "Database of Prompt Gamma Rays from Slow Neutron Capture for Elemental Analysis," IAEA, Vienna, 2007.

Krenn, R. and G. Hirzinger, "Scm - A soil contact model for multi-body system simulations." *11th European Regional Conference of the International Society for Terrain-Vehicle Systems*, Bremen, 2009.

Lange, C. et al., "Baseline Design of a Mobile Asteroid Surface Scout (MASCOT) for the Hayabusa 2 Mission." *7th Interplanetary Probe Workshop*, Barcelona, 2010.

Lee, S., "High reliability-low noise radionuclide signature identification algorithms for border security applications," University of Utah, Salt Lake City, 2016.

Mangwandi C., Y.S. Cheong, M.J. Adams, M.J. Hounslow, A.D. Salman, "The coefficient of restitution of different representative types of granules," *Chemical Engineering Science*, vol. 62, pp. 437–450, 2007.

McNutt, L. et al, "Near-Earth Asteroid Scout," 2014 [Online]. Available: http://ntrs.nasa.gov/ archive/nasa/casi.ntrs.nasa.gov/20140012882.pdf

Moss, C.E., K.D. Ianakiev, T.H. Prettyman, M.K. Smith and M.R. Sweet, "Multi-element, large-volume CdZnTe detectors," *Nuclear Instruments and Methods in Physics Research Section A: Accelerators, Spectrometers, Detectors and Associated Equipment*, vol. 458, no. 1-2, pp. 455–460, 2001.

Park, R.S., R.A. Werner, S. Bhaskaran, "Estimating small-body gravity field from shape model and navigation data," *J. Guidance, Control and Dynamics*, vol. 33, pp. 212–221, 2010.

Pavone, M. et al. "Spacecraft/Rover Hybrids for the Exploration of Small Solar System Bodies," *NASA NIAC Phase I Study: Final Report*. Stanford University. 30 September 2012.

Pravec, P., A.W. Harris, B.D. Warner, "NEA rotations and binaries," In *IAU Proc. Symp., 236th*, ed. G.B.Valsecchi and D. Vokrouhlicky, pp. 167–176. Cambridge, UK: Cambridge Univ. Press, 2007.

Prettyman, T.H. et al., "Dawn's Gamma Ray and Neutron Detector," *Space Sci. Rev.*, vol. 163, pp. 371–459, 2011.

Prokesch, M., "CdZnTe for Gamma and X-Ray Applications," in *Solid-State Radiation Detectors*, CRC Press, 2015, pp. 17–48.

Reid, R. et al., "Contact Dynamics of Internally-Actuated Platforms for the Exploration of Small Solar System Bodies," *12th International Symposium on Artificial Intelligence, Robotics and Automation in Space (i-SAIRAS2014),* Saint-Hubert, Canada, 2014.

Reill, J. et al., "MASCOT – Asteroid Lander With Innovative Mobility Mechanism," *13th Symposium on Advanced Space Technologies in Robotics and Automation*, Noordwijk, The Netherlands. June 2015.

Rieder, R., H. Wanke, T. Economou and A. Turkevich, "Determination of the chemical composition of Martian soil and rocks: The alpha proton X ray spectrometer," *Journal of Geophysical Research*, vol. 102, no. E2, pp. 4027–4044, 1997.

Schindler, K., C.A. Thomas, V. Reddy, A. Weber, S. Gruska and S. Fasoulas, "PANIC – A surface science package for the in situ characterization of a near-Earth asteroid," *Acta Astronautica*, vol. 68, no. 11, pp. 1800–1810, 2011.

Schlesinger, T.E, J.E. Toney, H. Yoon, E.Y. Lee, B.A. Brunett, L. Franks and R.B. James, "Cadmium zinc telluride and its use as a nuclear radiation detector material," *Mater. Sci. Eng.: R*, vol. 32, no. 4, pp. 103, 2001.

Supulver, K.D., F.G. Bridges, D.N.C. Lin, "The coefficient of restitution of ice particles in glancing collisions: Experimental results for unfrosted surfaces," *Icarus*, vol. 113, pp. 188–199, 1995.

Tardivel, S., E. Canalias, M. Deleuze, A.T. Klesh, and D. Scheeres, "Landing MASCOT on Asteroid 1999 JU3: Solutions for Deploying Nanosats to Small Body Surface," *46th Lunar and Planetary Science Conference*, vol. 46, pp. 1182, 2015.

Ulamec, S. et al., "Hopper Concepts for Small Body Landers." *Journal of Advances in Space Research*, vol. 47, pp. 428–439, 2011.

Werner, R.A. and D. Scheeres, "Exterior gravitation of a polyhedron derived and compared with harmonic and mascon gravitation representations of asteroid 4769 castalia," *Celestial Mechanics and Dynamical Astronomy*, vol. 65, no 3, pp. 313–344, 1997.

Yoshimitsu, T. et al., "MINERVA Rover Which Became an Artificial Solar Satellite." *20th Annual AIAA/USU Conference on Small Satellites*. 2006.

Yoshimitsu, T. et al., "Micro-Hopping Robot for Asteroid Exploration." *Acta Astronautica*, vol. 52, pp. 441–446, 2003.

Standard NAA Facility
(room size)
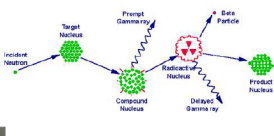
Instrument Study:
- Sensors
- Neutron sources
- Instrument design/packaging

TiO$_2$ Nanotubular template (inset shows the side view of the nanotubes) (left) and CZT nanowires (right) fabricated at University of Utah for nanosensor

Miniature Instrument using nanostructured sensors
(Sensor: chip size; Instrument: <1/2U)

Neutral source selection. Neutristor (left) CF252(right)

Mission/Spacecraft Design Study:
- nano-lander design
- landing technology
- surface operation
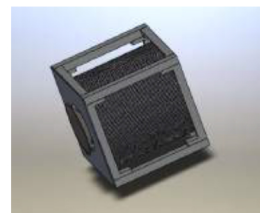
CubeSat based lander

CubeSat Lander Mission to Asteroids/Comets
(Lander: 1 to 2U; ~1kg)
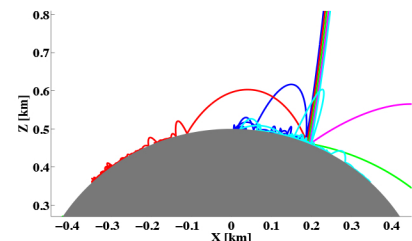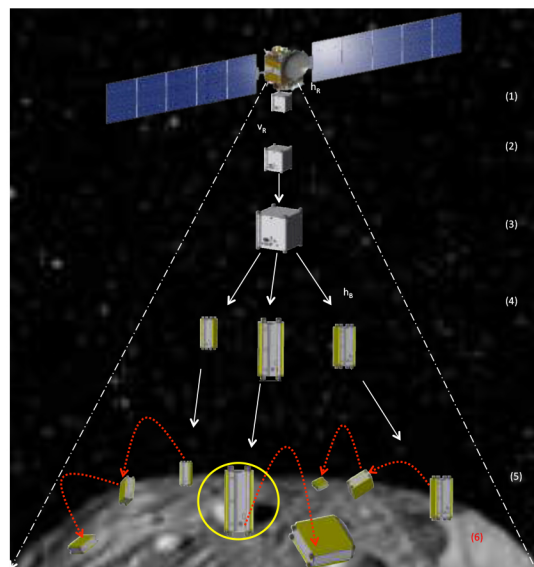
Uncontrolled descent & hopping landing

Figure I.1. Overview of NIAC concept, proposed study, and technology roadmap
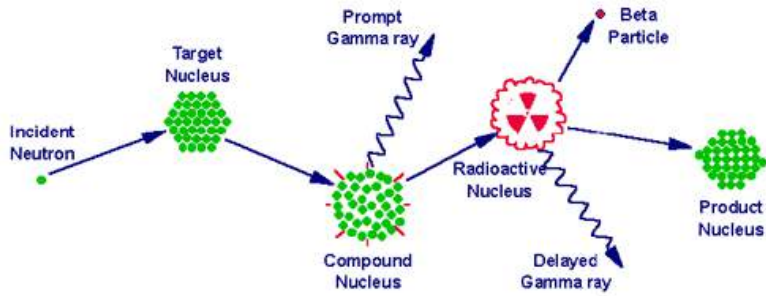
Figure II.1. NAA process. (Illustration from www.murr.missouri.edu)
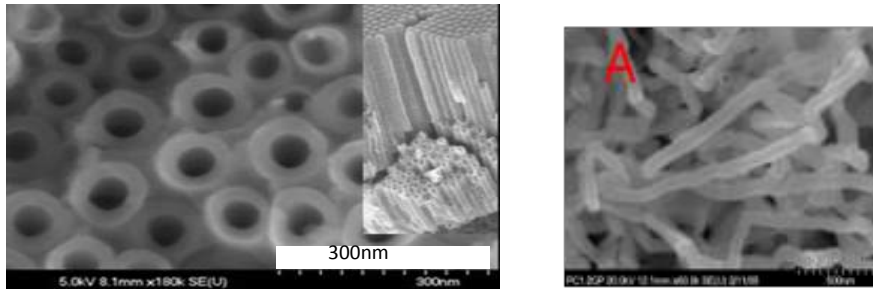
Figure II.2. TiO$_2$ Nanotubular template (inset shows the side view of the nanotubes) (left) and CZT nanowires (right) fabricated at University of Utah.
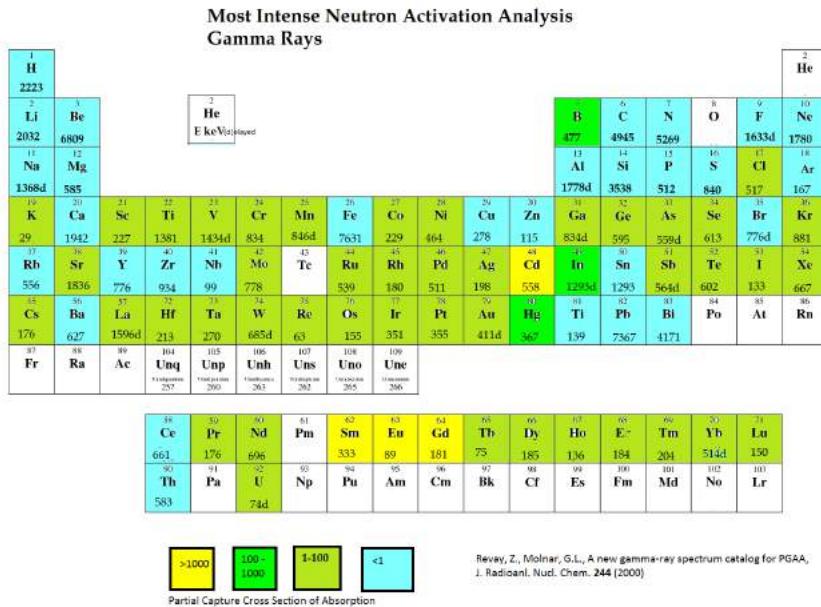
Figure II.3. Periodic table with partial capture section which represents the probability that a neutron will be absorbed and emit a gamma ray.
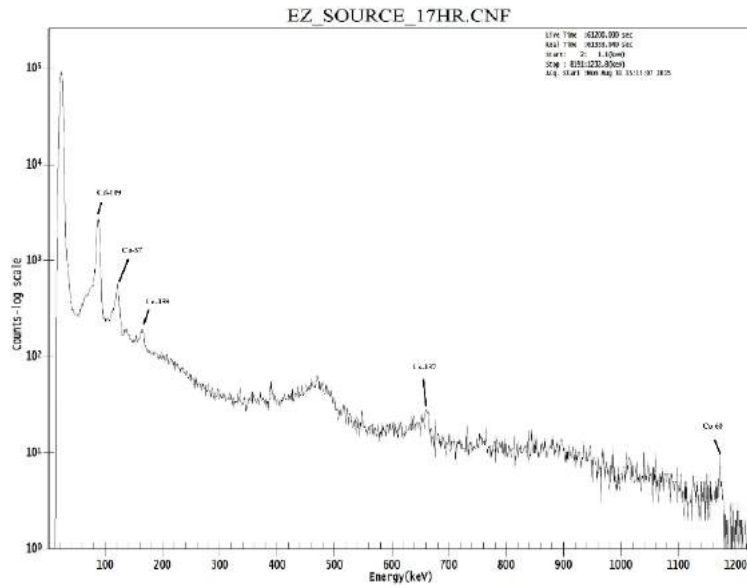
Figure II.4. Example of measured gamma ray spectrum using a 5mm CZT crystal
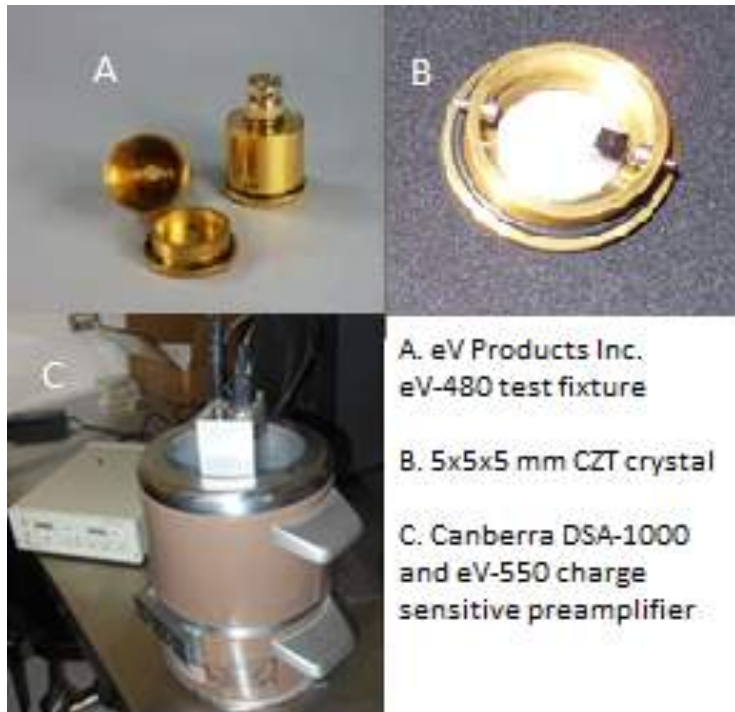
Figure II.5. Equipment setup for spectrometer grade 5 mm³ planar CZT crystal from eV Products Inc.
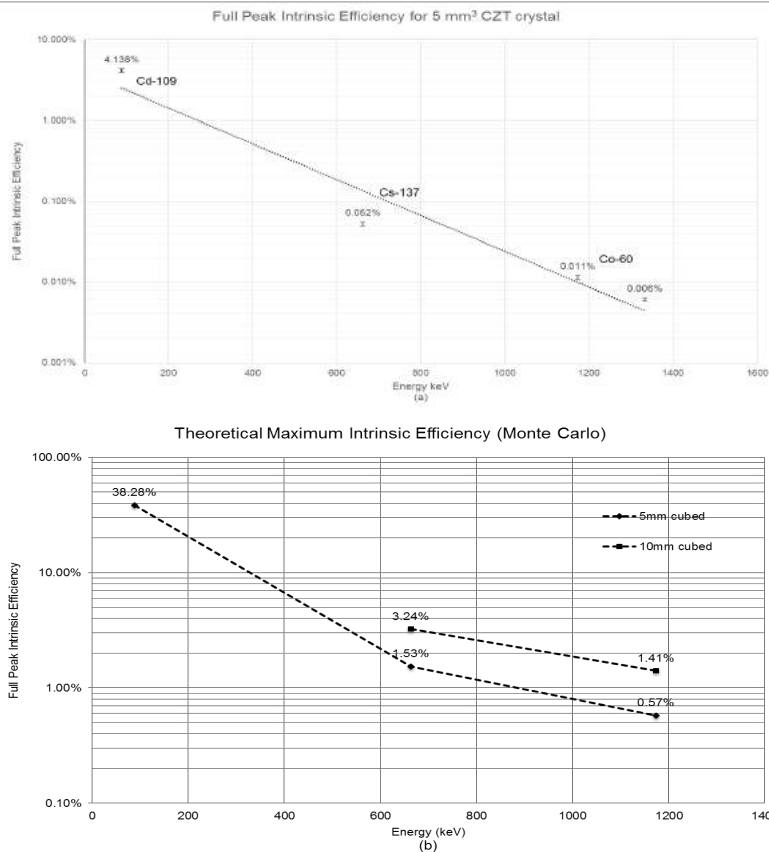
Figure II.6 (a)Full peak intrinsic efficiency measured from 5 mm cubes spectrometer grade CZT crystal using an eV Products eV-480 test fixture, eV-550 preamplifier, Canberra MCA, and GENIE 2000 data acquisition software. Photo-peak intrinsic efficiency decreases exponentially with gamma ray energy. (b)Maximum theoretical efficiency using GEANT4 Monte Carlo simulation for 5mm cubed and 10mm cubed CZT crystals.
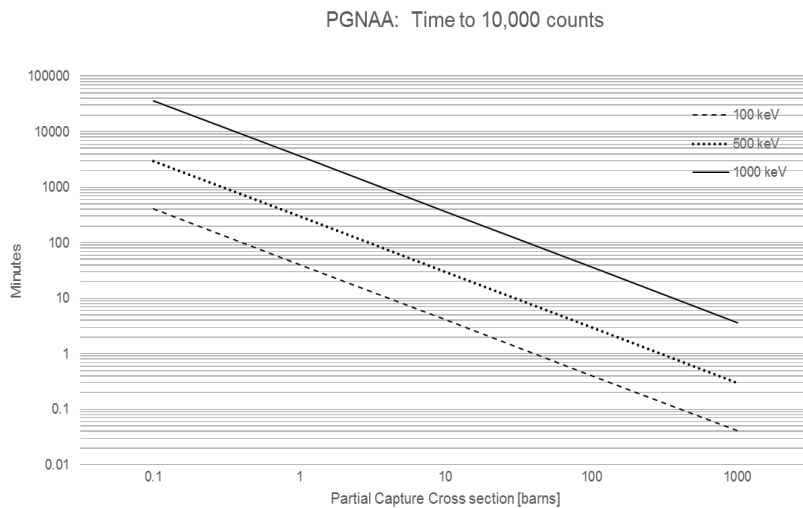
Figure II.7. Estimated PGNAA counting times for elements by thermal partial capture cross-section emitting gamma of energy E_γ. Calculations for Eq. 3 assumed a uniform thermal neutron flux of 10^6 cm^{-2}s^{-1}, 1 g of sample, a solid angle of 0.25 ster., and the theoretical maximum intrinsic full peak efficiency from Monte Carlo simulation. Counting time has a linear relationship to each factor in Eq. 3, thus a reduction of any factor by an order of magnitude results in a corresponding increase in counting time.

(a)

(b)
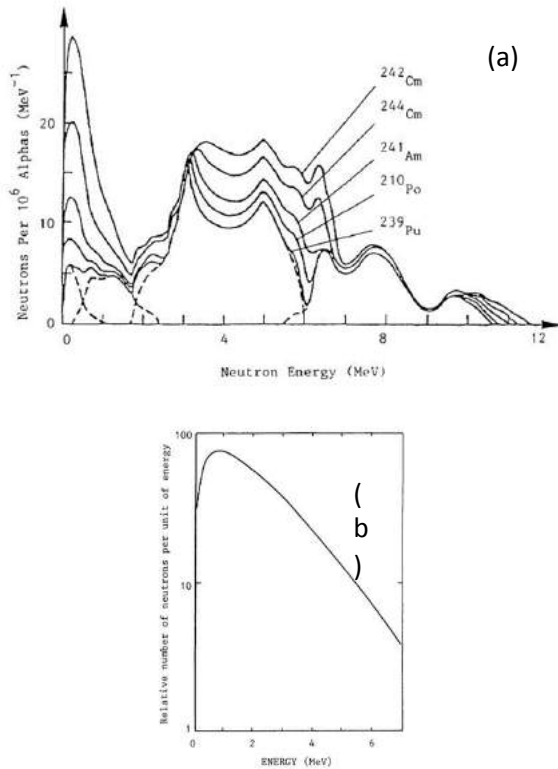
Figure II.8. (a) Neutron energy spectra for various mixed sources. (b) Neutron energy spectrum for Cf-252. [12]
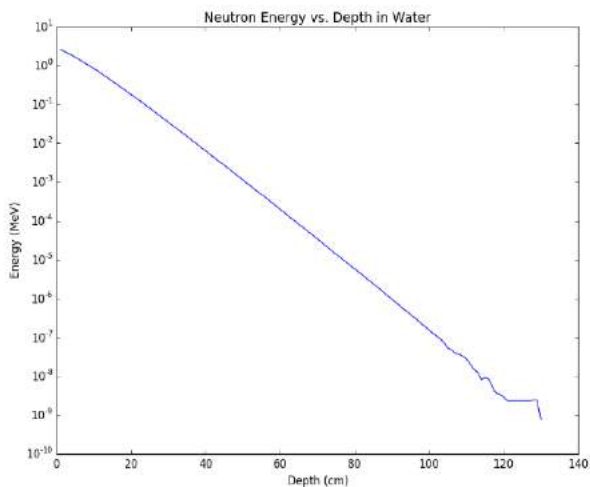
Figure II.9 MCNP computation of neutron penetration depth in a slab of water at 20C from an initial energy of 2.5 MeV. Thermal energies are reached at approximately 1 m.
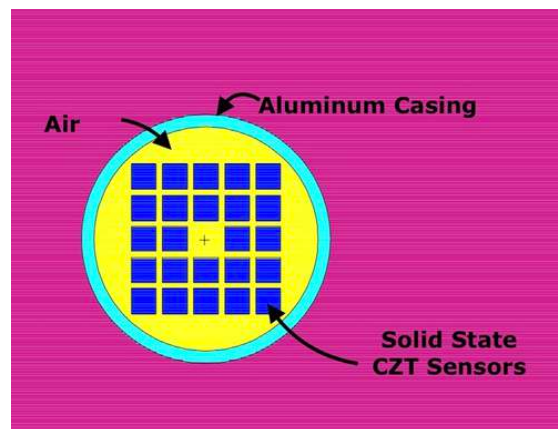
Figure II.10 Miniature instrument detector model developed in MCNP
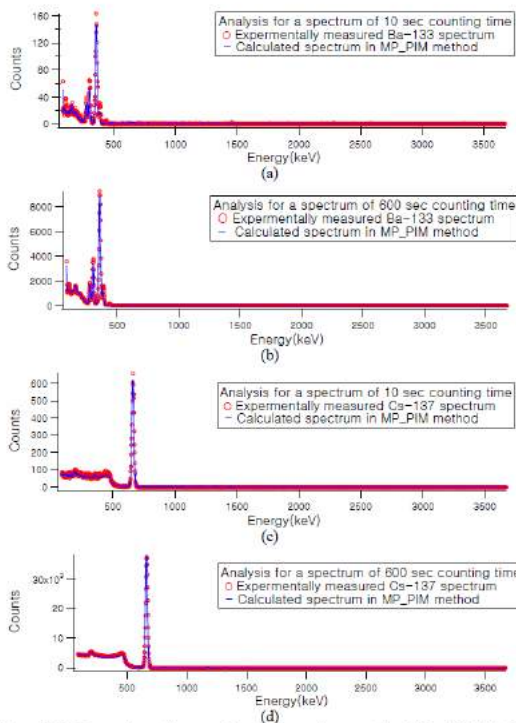
Figure 3.12. Comparison of measured and estimated spectra for: (a) Ba-133 with 10 sec counting time, (b) Ba-133 with 600 sec counting time, (c) Cs-137 with 10 sec counting time, (d) Cs-137 with 600 sec counting time.
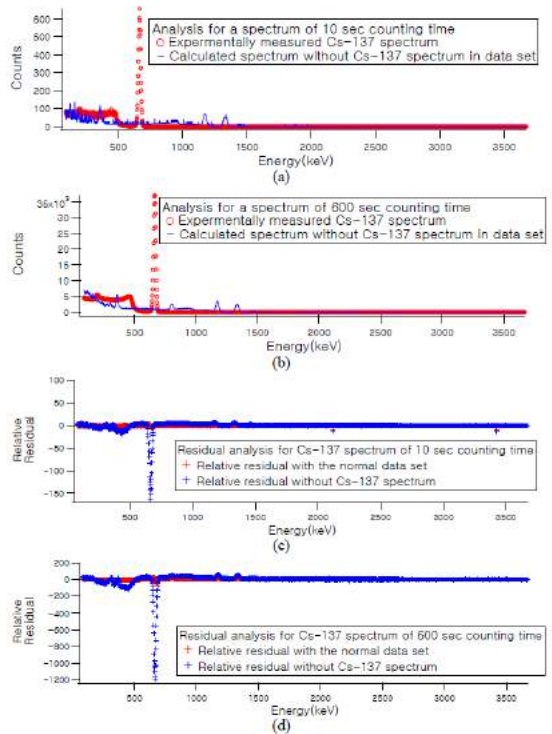
Figure 3.14. MP_PIM analysis of Cs-137 measured spectra without the Cs-137 computed spectrum in the data set (a) for 10 sec counting time, and (b) for the 600 sec counting time and relative residuals (c) for 10 sec counting time, and (d) for the 600 sec.

(b)

Figure II.11 (a) Comparison of measured spectra and computed spectra using Lee's MP_PIM algorithm for Ba-133 and Cs-137. (b) Residual analysis for Cs-137 using Lee's MP_PIM algorithm when the Cs-147 spectrum is not included in the computed spectrum. [9]

Table II.1. List of common radioisotope neutron sources. Included in the list is Sandia National Lab's "neutristor" source. The neutristor source can only be operated in microsecond pulses to prevent heating and out migration of target material.

Neutron Source	$^{241}AmBe$ [11]	$^{238}PuBe$ [12]	$^{239}PuBe$ [12]	$^{244}CmBe$ [12]	$^{226}RaBe$ [12]	^{252}Cf [12]	Neutristor [8]
Source Strength (n/s/g)	$7.59 * 10^6$	$5.08 * 10^7$	$1.2 * 10^5$	$3.30 * 10^8$	$1.48 * 10^7$	$2.28 * 10^{12}$	$\sim 1 * 10^9$ 2000 n/pulse $1pulse = 1\mu s$
Density or Size (g to cm³)	Am: $12 g/cm^3$ Be: $1.85 g/cm^3$	Pu: $19.8 g/cm^3$ Be: $1.85 g/cm^3$	Pu: $19.8 g/cm^3$ Be: $1.85 g/cm^3$	Cm: $13.5 g/cm^3$ Be: $1.85 g/cm^3$	Ra: $5.5 g/cm^3$ Be: $1.85 g/cm^3$	Cf: $15.1 g/cm^3$ $1g = 0.066 cm^3$	1.54 x 3.175 x 0.05 cm
Average Neutron Energy	4.2 MeV (11 max)	4.2-5 MeV (11 max)	4.2-5 MeV (10.5 max)	4.31 MeV (11.2 max)	3.6 MeV (13.2 max)	2.14 MeV (10+ max)	2.5-3 MeV (14 max)
Half-Life	458 y	89 y	24.36 y	18.1 y	1620 y	2.64 y	

Table II.2. Size and mass estimations for preliminary instrument design 1

Component	Volume (cm^3)	# of Items	Total	Material	Density (g/cm^3)	Mass (g)
Source	0.4	1	0.4	Cf	15.15	6.06
CZT Sensor	0.125	36	4.5	CZT	5.78	26.01
Circuit Housing	2.12	1	2.12	Aluminum	2.7	5.724
Main Housing	15.307	1	15.307	Aluminum	2.7	41.3289
IC Card						30
BNC Connectors/Wires						30
Power Supply	25	1	25		4	100
					Total:	239.1229

Table II.3. Size and mass estimations for preliminary instrument design 2.

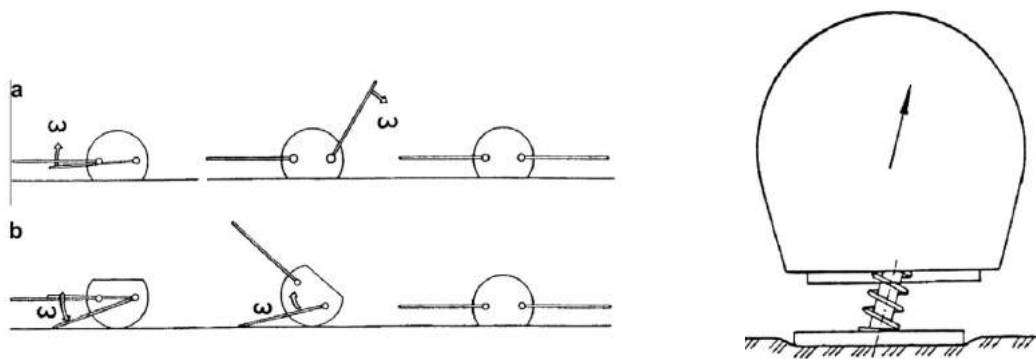| Component	Volume (cm^3)	# of Items	Total	Material	Density (g/cm^3)	Mass
Cylindrical Housing	51.05	1	51.05	Aluminum	2.7	137.835
Dome Cap	33.25	1	33.25	Aluminum	2.7	89.775
CZT Sensor	0.125	12	1.5	CZT	5.78	8.67
Moderator Slab	6.28	7	43.96	Polyethyline	0.96	42.2016
Source	0.4	1	0.4	Cf	15.15	6.06
IC Card		1				30
BNC Connectors/Wires						30
Power Supply	25	1	25		4	100
					Total:	444.5416

Figure III.1. PrOP-F Uprighting Mechanism (left) and PrOP-F Piston Mechanism (right)
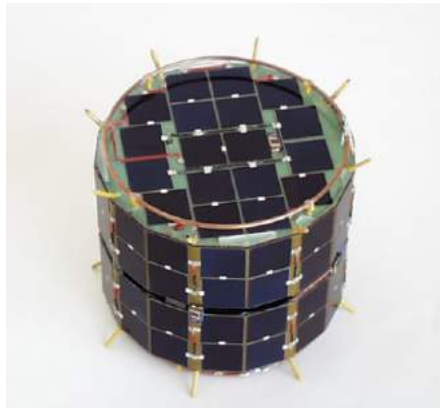

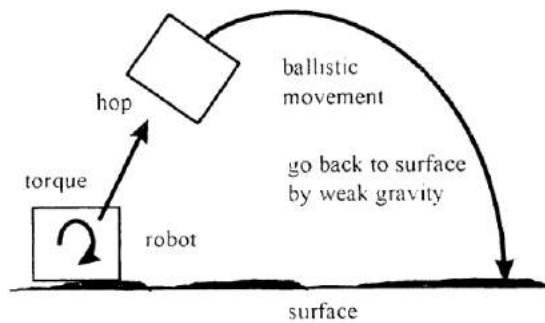**Figure III.2.** MINERVA Probe (w/ cover and solar panels) [Yoshimitsu et al. 2006]

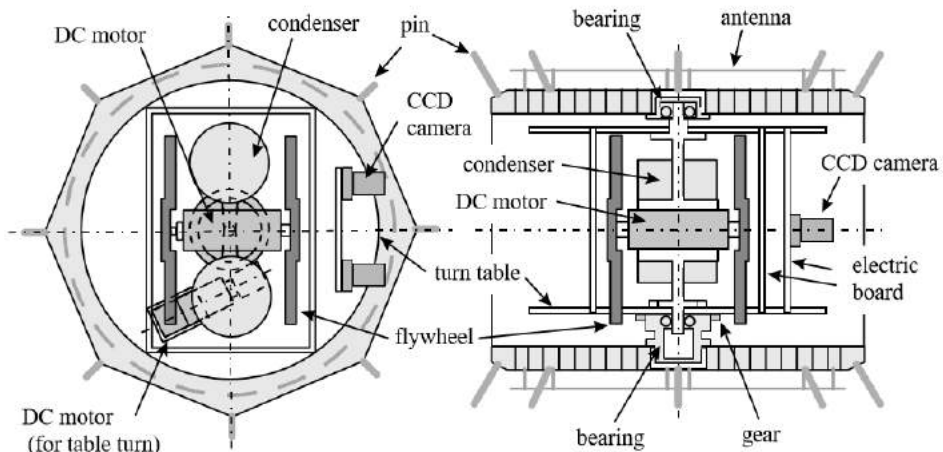**Figure III.3.** MINERVA "hop" motion from torque generation [Yoshimitsu et al. 2003]

Figure III.4 MINERVA Flywheel Mobility Mechanism [Yoshimitsu, T. et al. 2003]

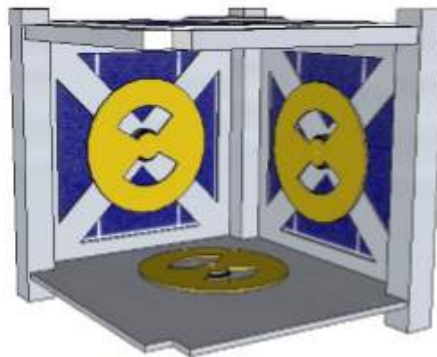**Figure III.5.** Hedgehog prototype I (payload and solar panels not included) [Reid, R. et al. 2014]

Figure III.6 Three orthogonal flywheel configuration (payload and external features not shown) [Pavone, M et al. 2012]
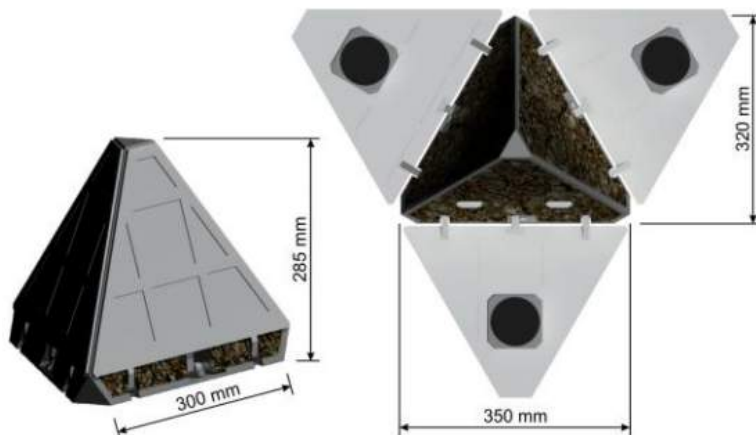
Figure III.7. PANIC tetrahedron lander design
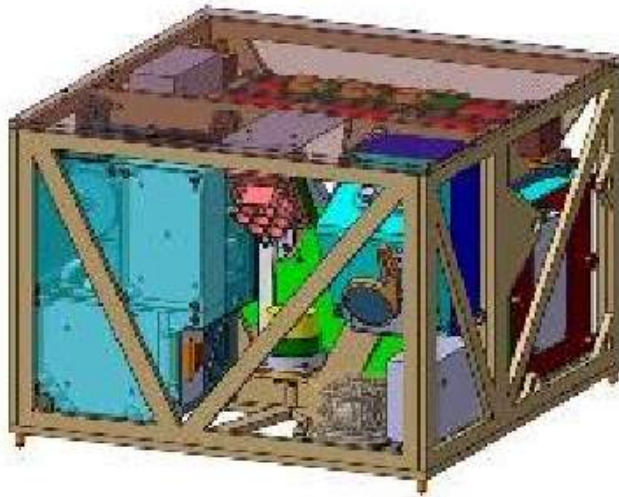
Figure III.8 CAD Model of Internal Configuration of MASCOT [Tardivel, S. et al 2015]
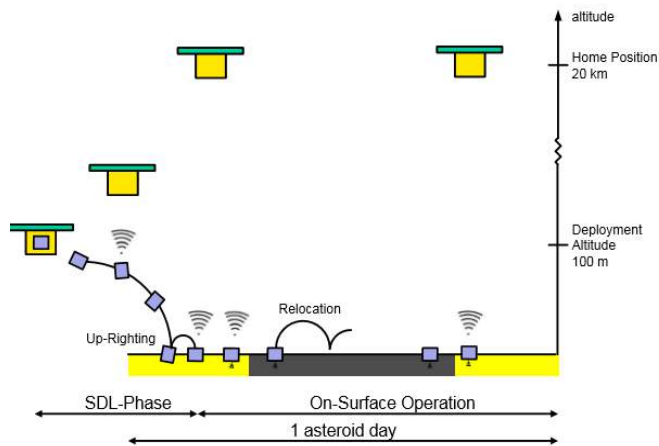
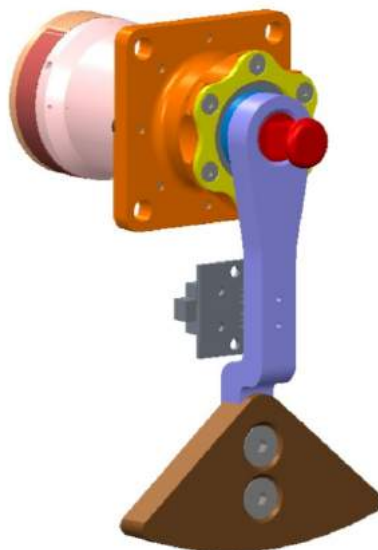**Figure III.9** Landing schematic for deployment of MASCOT by Hayabusa II [Reill, J. et al. 2015]

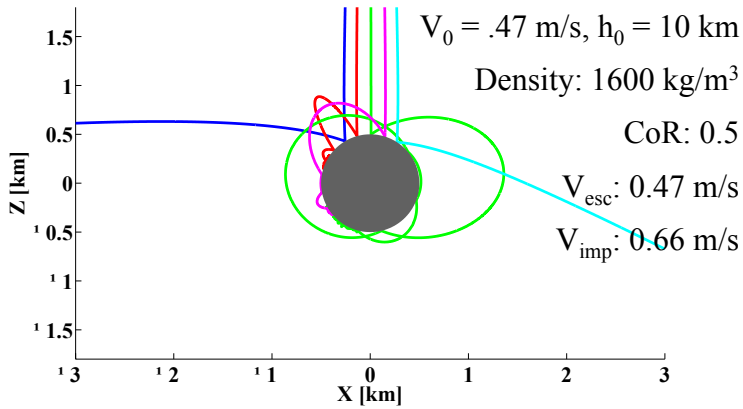**Figure III.10.** CAD Diagram of eccentric momentum pulse arm to installed on MASCOT [Grundmann, J. et al. 2014]

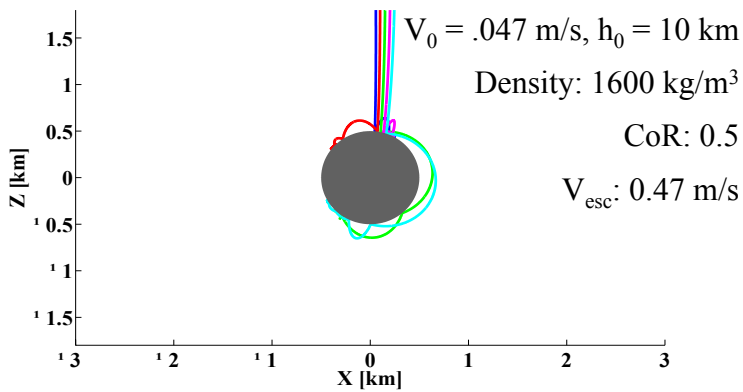**Figure III.11:** Lander rebound trajectories on 1 km asteroid, $v_0 = .47$ m/s

Figure III.12: Lander rebound trajectories on 1 km asteroid, $v_0 = .047$ m/s

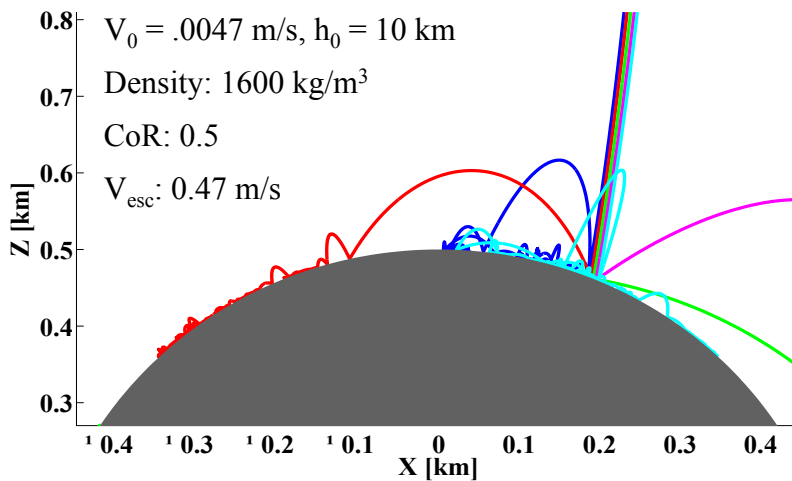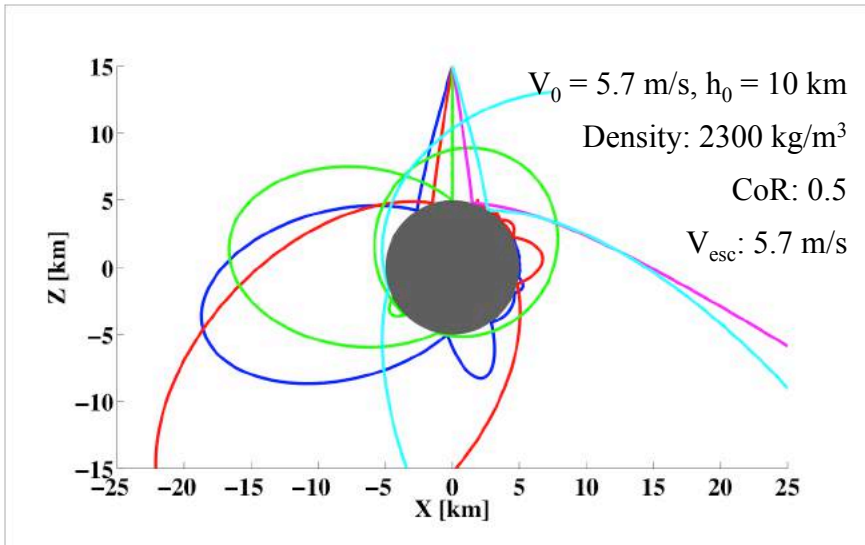**Figure III.13:** Lander rebound trajectories on 1 km asteroid, $v_0 = .0047$ m/s

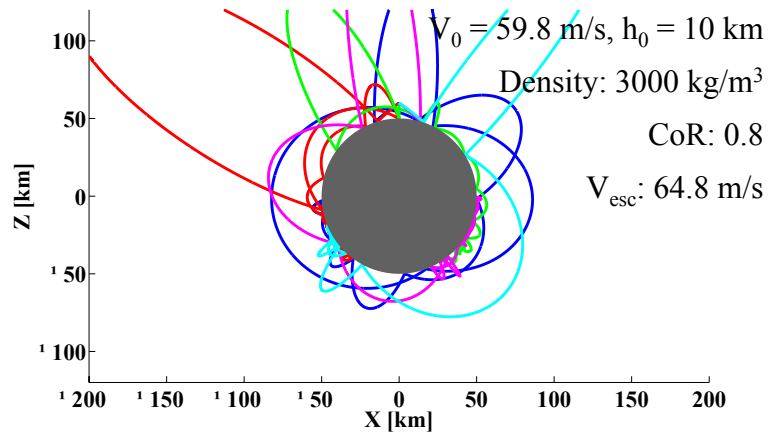**Figure III.14.** Lander rebound trajectories on 10 km asteroid, $v_0 = 5.7$ m/s

Figure III.15. Lander rebound trajectories on 100 km asteroid, $v_0 = 59.8$ m/s
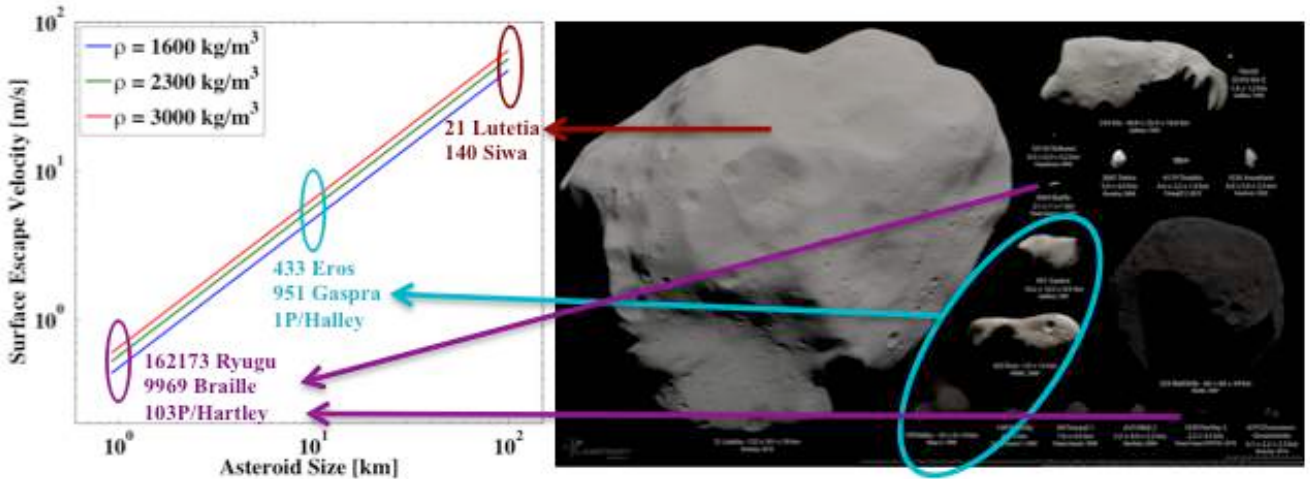
Figure III.16. Left: Surface escape velocity vs. asteroid size, one of the limiting factors on the feasibility of the proposed mission scenario. Right: Small bodies visited by spacecraft, to scale [Lakdawalla 2014]

Table III.1. Comparison of previous missions or designs on asteroid/comet landing with the design considered in this study. *values listed were for planned mission, actual values were different which caused failure to land. +proposed value ranges/mechanism for the 2U

Lander	Mass (kg)	Rough Volume (cm³)	Release Velocity (cm/s)	Release Altitude (m)	Escape Velocity (cm/s)	Mobility Mechanism
PrOP-F	41.2	900000π (~2800000)	300-350	1000-2000	1140	2 lever arms + piston
MINERVA	0.59	360π (~1130)	5*	70*	30-35	1 flywheel on turntable
PANIC	12	5000	n/a	n/a	n/a	1 lever arm
Hedgehog	10	62500π/3 (~65450)	n/a	n/a	n/a	3 normal flywheels
MASCOT	10	18000	3-4	100	32-36	1 eccentric arm
Philae	100	800000	18.67	20500	44 - 100	n/a
2U Nanolander+	< 5	2000	5-10	< 200	30-50	1 flywheel

Table III.2: Summary of a small asteroid lander capture

Diameter:	1 km	Initial altitude:	10 km		Rotation Period:	7.6 hrs	
		Density [kg/m^3]	3000		Density [kg/m^3]	3000	
Surface Vesc [m/s]	0.65	Coeff Restitution	0.8	Vi/Vesc	Coeff Restitution	0.5	Vi/Vesc
		Vi Limit [m/s]	0.13	0.20	Vi Limit [m/s]	0.65	1.00
		Density [kg/m^3]	2300		Density [kg/m^3]	2300	
Surface Vesc [m/s]	0.57	Coeff Restitution	0.8	Vi/Vesc	Coeff Restitution	0.5	Vi/Vesc
		Vi Limit [m/s]	0.11	0.20	Vi Limit [m/s]	0.57	1.00
		Density [kg/m^3]	1600		Density [kg/m^3]	1600	
Surface Vesc [m/s]	0.47	Coeff Restitution	0.8	Vi/Vesc	Coeff Restitution	0.5	Vi/Vesc
		Vi Limit [m/s]	0.09	0.20	Vi Limit [m/s]	0.47	1.00

Table III.3: Summary of an intermediate asteroid lander capture

Diameter:	10 km	Initial altitude:	10 km		Rotation Period:	7.6 hrs	
		Density [kg/m^3]	3000		Density [kg/m^3]	3000	
Surface Vesc [m/s]	6.5	Coeff Restitution	0.8	Vi/Vesc	Coeff Restitution	0.5	Vi/Vesc
		Vi Limit [m/s]	4.2	0.65	Vi Limit [m/s]	6.6	1.02
		Density [kg/m^3]	2300		Density [kg/m^3]	2300	
Surface Vesc [m/s]	5.7	Coeff Restitution	0.8	Vi/Vesc	Coeff Restitution	0.5	Vi/Vesc
		Vi Limit [m/s]	3.4	0.60	Vi Limit [m/s]	5.7	1.01
		Density [kg/m^3]	1600		Density [kg/m^3]	1600	
Surface Vesc [m/s]	4.7	Coeff Restitution	0.8	Vi/Vesc	Coeff Restitution	0.5	Vi/Vesc
		Vi Limit [m/s]	2.6	0.55	Vi Limit [m/s]	4.7	1.01

Table III.3: Summary of a large asteroid lander capture

Diameter:	10 km	Initial altitude:	10 km		Rotation Period:	7.6 hrs	
		Density [kg/m^3]	3000		Density [kg/m^3]	3000	
Surface Vesc [m/s]	65	Coeff Restitution	0.8	Vi/Vesc	Coeff Restitution	0.5	Vi/Vesc
		Vi Limit [m/s]	59.8	0.92	Vi Limit [m/s]	66.3	1.02
		Density [kg/m^3]	2300		Density [kg/m^3]	2300	
Surface Vesc [m/s]	57	Coeff Restitution	0.8	Vi/Vesc	Coeff Restitution	0.5	Vi/Vesc
		Vi Limit [m/s]	51.3	0.90	Vi Limit [m/s]	57.6	1.00
		Density [kg/m^3]	1600		Density [kg/m^3]	1600	
Surface Vesc [m/s]	47	Coeff Restitution	0.8	Vi/Vesc	Coeff Restitution	0.5	Vi/Vesc
		Vi Limit [m/s]	41.4	0.88	Vi Limit [m/s]	47.0	1.00